METHODS OF CALCULATING AERODYNAMIC LOADS ON AIRCRAFT STRUCTURES: PART II - NONLINEAR EFFECTS

THOMAS E. CHAMBERLAIN

MASSACHUSETTS INSTITUTE of TECHNOLOGY

*** Export controls have been removed ***

FOREWORD

This publication constitutes the second part of a three-part final report prepared under USAF Contract No. AF 33 (615)-2291. The contract was initiated under Project No. 1367, Task No. 136715. The work was performed at the Aerophysics Laboratory, Massachusetts Institute of Technology, for the Air Force Flight Dynamics Laboratory, Research and Technology Division with most calculations performed at the M. I. T. Computation Center. Mr. Charles E. Jobe monitored the project for the Air Force. The M. I. T. faculty supervisor was Prof. Morton Finston, and Dr. Leon H. Schindel was Principal Investigator.

This report covers work conducted from October 1964 to April 1966.

The manuscript of this report was released by the author April 1966 for publication as a RTD Technical Report.

This technical report has been reviewed and is approved.

Francis K. Janik, Jr.
Chief, Theoretical Mechanics Branch
Structures Division

ABSTRACT

A method is presented for analysis of the nonlinear aerodynamics of slender configurations with vortex separation. Primary emphasis is on the nonlinear component of the aerodynamic characteristics. The theory is intended to be mathematically tractable yet give results of acceptable accuracy.

A technique for analyzing the nonlinear aeroelastic problem is given followed by a method for obtaining the nonlinear aerodynamics of wings, bodies, and their combinations. Comparisons with experiment are provided.

The experimental comparisons with the wing results indicate that the theory overestimates the nonlinear forces at high angles of attack. The results indicate directions for further research.

CONTENTS

ILLUSTRATIONS

ILLUSTRATIONS (Continued)

vi

SYMBOLS

a	semi-major axis of elliptic body
A	wing planform area
A_{ij}	aerodynamic influence coefficient
b	wing local semi-span
C_{ij}	structural influence coefficient
C_L	total lift coefficient
C_p	pressure coefficient
C_m	pitching moment coefficient (about the nose)
F	force
h	elliptic parameter
$[I]$	identity matrix
i	$\sqrt{-1}$
$I.P.$	imaginary part of complex number
k	elliptic parameter
K	source strength
ℓ	body length
M_∞	free stream Mach number
$N(x)$	normal force up to station x
P	pressure
q_∞	dynamic pressure $= \frac{\rho}{2} U_\infty^2$
r	circular body radius
$R.P.$	real part of complex number
S_i	velocity due to a source
S	local semi-span, including body

SYMBOLS (Continued)

s'	transformed local semi-span
U_∞	free stream velocity
u	x-component of the velocity perturbation
v	y-component of the velocity perturbation
V_g^*	complex flow velocity relative to vortex
w_η	vertical component of velocity in cross-flow plane
ω	z-component of velocity perturbation
W_g	complex velocity at the vortex
x	streamwise coordinate
X	complex variable, circle plane = $y + iz$
X_0	vortex location
X_1	image vortex location
y	spanwise coordinate
z	vertical coordinate
α	angle of attack
α_0	average body angle of attack
α_i	local wing slope
α_i^0	local "rigid" wing slope
β	$\sqrt{1 - M_\infty^2}$
Γ	vortex strength
δ	cone semi-vertex angle
ϵ	wing semi-vertex angle
$\mathscr{S}$	complex variable, elliptic plane = $\xi + i\eta$
$\mathscr{S}_0, \mathscr{S}_1$	vortex locations, wing and body

SYMBOLS (Concluded)

x_0', y_1' separation points, wing and body

η vertical coordinate, elliptic plane

θ complex variable $y + iz$

θ_0, θ_1 vortex locations, wing and body

θ_0', θ_1' separation point locations

Λ leading edge sweep angles

λ nondimensional vortex strength

ρ density

σ complex variable $y' + iz'$

ϕ complex potential function

$\phi_{(3-D)}$ three-dimensional complex potential

φ velocity potential

ψ stream function

SECTION I

INTRODUCTION

Flight technology progress has brought about increasingly higher speeds in a trend which will certainly continue. These higher speeds generally require slender aircraft configurations. Because of their slender nature, these aircraft may experience aerodynamic forces which have a significantly nonlinear variation with angle of attack, in contrast with the higher aspect ratio aircraft. While mathematical techniques for analyzing the high aspect ratio "linear" problem are reasonably complete, methods for calculating the nonlinear forces on slender aircraft are still in the developmental stage. In this report, some recent procedures will be described for calculating nonlinear aerodynamic forces on elastic lifting configurations.

The report is concerned with three configurations: wings, bodies, and wing-body combinations. The theoretical development of the aerodynamics of each configuration type is given, followed by comparisons with experiment. An approach toward calculating aerodynamic influence coefficients accounting for nonlinearity is first discussed preceding the theoretical development of the aerodynamics.

Nonlinear lift on delta wings caused by vortex separation from the leading edges was treated by Brown and Michael[3]. Subsequently, Bryson[4] solved the corresponding problem for circular cones and cylinders. The present results are based on an extension by Schindel[1] of these methods which permits application to wings and bodies of more general shape.

In these analyses, nonlinear forces are attributed to the effects of flow separation on the lee side of wings and bodies. The separating vortex sheets are assumed to roll up into concentrated vortices which are connected to the separation points by feeding sheets (e.g., Fig. 2). Requirements that each vortex and feeding sheet be force free and that separation exist at prescribed locations determine the vortex strengths and positions.

It is important to note that this report is primarily concerned with the nonlinear component of the aerodynamics considered. In application of the material prescribed herein, more accurate linear theories[5] should be coupled with the slender body analysis of the nonlinear effects.

1

SECTION II

NONLINEAR AEROELASTICITY

The aerodynamic analyses of flight vehicles are generally made with the assumption that the configurations are rigid. In practice, however, these vehicles are not rigid and the solutions must be adapted to allow analysis of this situation. For linear theory, the adaptation is straight forward; the linear property allows the calculation of aerodynamic influence coefficients defining the aerodynamic characteristics of the wing for an arbitrary angle of attack distribution. Nonlinearity due to flow separation, however, introduces a degree of complexity into the analysis. The need for a linear analysis still remains but it must include the nonlinear feature. It is the purpose of this section to present a method which attempts to meet this requirement. The development of the method is oriented to a thin wing; however, the basic concept appears applicable to bodies and wing-body combinations.

Matrix methods are generally used in the aeroelastic analysis of wings and bodies. If, for example, ΔP_j represents the pressure difference acting across a small area of a wing, then the following matrix equation relates the pressure distribution to the distribution of angle of attack.

$$\left[\Delta P_j\right] = \left[A_{ij}\right]\left[\alpha_i\right] \qquad (1)$$

where α_i is the angle of attack or slope of the ith wing area and $\left[A_{ij}\right]$ is the aerodynamic matrix. The element A_{ij} of the aerodynamic matrix represents the pressure difference at j due to a unit angle of attack at area i .

The pressure difference will cause a structural deformation of the wing surface which may be represented by the following matrix equation.

$$\left[\alpha_i\right] - \left[\alpha_i^\circ\right] = \left[C_{ij}\right]\left[\Delta P_j\right] \qquad (2)$$

In this equation, $\left[\alpha_i\right] - \left[\alpha_i^\circ\right]$ is the change in wing slope due to structural deformation under load, and C_{ij} is a structural matrix giving the slope change at area i due to a pressure difference at area j .

Solution of the matrix equation gives the load distribution on a flexible wing.

$$[\Delta P_j] = \left[[I] - [A_{ij}][C_{ij}]\right]^{-1}[A_{ij}][\alpha_i^\circ] \qquad (3)$$

where $[I]$ is the identity matrix.

The foregoing process assumes a linear relation between pressure and angle of attack and between load and deflection. In order to account for a nonlinear relation between angle of attack and aerodynamic load, it is first necessary to revise the aeroelastic equations. If Eq. (1) is replaced by the expression

$$[\Delta P_j] = [\Delta P_j^\circ] + [A_{ij}][\alpha_i - \alpha_i^\circ] \qquad (4)$$

where $[\Delta P_j]$ is a matrix giving the undeformed wing pressure distribution including the nonlinear component, then each element of the new aerodynamic matrix $[A_{ij}]$ gives a relation between the pressure distribution and perturbation in angle of attack about the corresponding rigid wing local angle of attack, α_i° (Fig. 1). For this case the final load distribution becomes

$$[\Delta P_j] = \left[[I] - [A_{ij}][C_{ij}]\right]^{-1}\left\{[A_{ij}][\alpha_i - \alpha_i^\circ] + [\Delta P_j^\circ]\right\} \qquad (5)$$

In this equation, ΔP_j° is obtained by combining a suitable linear theory with the nonlinear theory described in the following section. The determination of the aerodynamic influence coefficients, A_{ij} will be described first.

The selected method is intended to optimize the combination of accuracy and calculation ease. The approach is to multiply each linear influence coefficient by a corresponding factor which incorporates the nonlinear effect. In order to determine the form of this factor it is necessary to give some consideration to the aerodynamic fundamentals of the problem.

On the basis of strictly linear theory, the magnitude of a pressure perturbation at location j due to a deflection at location i is directly proportional to the deflection. To the degree of accuracy inherent in the nonlinear aerodynamic analysis of the following sections, it appears allowable to relate the influence of one location on the pressure at another to the pressure changes induced at the influencing location rather than the deflection itself. Hence, the factor multiplying the linear influence coefficient will involve some ratio of the nonlinear and linear pressure slopes at the location i. These slopes are adequately obtained by analyzing the rigid wing at the angle of attack of interest.

Additional inspection of the nonlinear aspects of the problem are required before the method of analysis can be formally specified. It should be noted that the nonlinearity is primarily due to rather large regions of circulation above the wing. The strength (and position) of this circulation

4

is a consequence of the flow separation mechanics at the chordwise sta-
tions upstream of the point of interest. The nonlinear pressures at a
location are due to the characteristics of the circulation at the concerned
chordwise station. It is here necessary to observe that since the non-
linear effect enters only through the existence of the circulation, a
structural deformation can only induce nonlinear effects in the downstream
direction. Thus it is found that the subsonic upstream aerodynamic in-
fluence coefficient will encompass only linear effects and must be so rep-
resented in the selected analysis.

On the basis of the foregoing discussion, the mathematical repre-
sentation of the influence coefficient may now be formulated.

$$\left[A_{ij}\right] = \left[A_{ij}\right]_L \left[\frac{dC_{p_i}}{d\alpha}\right]_{N.L.} \left[\frac{dC_{p_i}}{d\alpha}\right]_L^{-1} \qquad ; \text{ downstream influence}$$

$$\left[A_{ij}\right] = \left[A_{ij}\right]_L \qquad\qquad\qquad\qquad\qquad\qquad ; \text{ upstream influence}$$

(6)

In the above relations, $\left[A_{ij}\right]_L$ is the linear aerodynamic influence co-
efficient matrix which may be obtained through use of the methods of Ref. 5
with some minor alterations. The nonlinear pressure coefficients are to
be obtained from the methods of the following section and Ref. 5. The com-
putation procedure for obtaining $\left[dC_{p_i}/d\alpha\right]_{N.L.}$ is cumbersome and will re-
quire a machine solution.

SECTION III

THE AERODYNAMICS OF SLENDER CONFIGURATIONS

A method for nonlinear aeroelastic analyses was presented in the preceding section. Part of the information needed for the method's application is comprised of the aerodynamic influence coefficients in a given flight situation. This section is intended to present an approach toward calculating these coefficients.

The section has two objectives. The first is to present the theory while the second is to compare theoretical calculations with experiment. It is also noted that the nonlinear aerodynamics component is of prime importance in this report; experimental comparisons are therefore intended to appraise only the accuracy of the nonlinear component.

Three distinct configurations are considered: wing-alone, body alone, and wing-body combinations. Each is discussed separately in detail.

A. THEORETICAL FOUNDATION

The considered problem is that of steady potential flow about slender configurations with vortex separation. This section is concerned with the mathematical formulation of the problem. Discussed below are the governing differential equation, corresponding boundary conditions, and vortex sheet model to be used. In the subsequent development, the slender body theory gives both linear and nonlinear aerodynamic forces; however, as previously discussed, more accurate linear theories should be coupled with the nonlinear results in actual application.

1. Governing Equation

The flow field consists of a slightly perturbed mainstream about a slender body. The governing equation of motion is the linearized equation

$$(1-M_\infty^2)\,\phi_{xx} + \phi_{\xi\xi} + \phi_{\eta\eta} = 0 \tag{7}$$

where M_∞ is the free stream Mach number, ϕ is the disturbance velocity potential, and x, ξ, and η are Cartesian coordinates fixed to the configuration. The orientation of the system is such that x coincides with a characteristic longitudinal axis and η is in the axis-free stream plane (Fig. 2). For sufficiently slender configurations, the term $(1-M_\infty^2)\,\phi_{xx}$ may be neglected and Eq. (7) becomes

7

$$\phi_{\xi\xi} + \phi_{\eta\eta} = 0 \tag{8}$$

which is the basic equation of slender body theory.

2. Boundary Conditions

The boundary conditions imposed on Eq. (8) are that disturbances vanish at infinity and that fluid velocities normal to configuration surfaces match the surface velocity. It is also generally required that the flow field pressure distribution be continuous; however, as discussed below, this condition is relaxed to simplify the problem.

3. Vortex Model

A simple model of the separated vortex sheet above a highly pitched slender body replaces the vortex sheet by a vortex core plus a "feeding" sheet extending to the separation point[3,6,7,8] (see Fig. 2). The strength and location of the vortex cores are obtained from the solution for the flow about this model. One of the two necessary conditions for solution is that a cross flow stagnation point exist at the given separation point. The second is that the vortex system (core plus feeding sheet) be force free.

The second condition may be formulated as follows. In complex variable notation $\mathscr{S} = \xi + i\eta$ with η in the vertical direction, the force on the feeding sheet is given by $\rho U_\infty \frac{d\Gamma_o}{dx}(\mathscr{S}_o - \mathscr{S}_o')i$ where Γ_o is the vortex strength, and $\mathscr{S}_o$ and $\mathscr{S}_o'$ are the vortex core and flow separation point locations respectively. The force on the vortex has the form $\rho\left[W_{\mathscr{S}_o} - U_\infty \frac{d\mathscr{S}_o}{dx}\right]\Gamma_o i$ where $W_{\mathscr{S}_o}$ is the cross-flow velocity at the vortex. Consequently, the condition for a force free vortex system is

$$U_\infty \frac{d\Gamma_o}{dx}(\mathscr{S}_o - \mathscr{S}_o') - V_{\mathscr{S}_o}^{*}\,\Gamma_o = 0 \tag{9}$$

where $V_{\mathscr{S}_o}^{*} = W_{\mathscr{S}_o} - U_\infty \frac{d\mathscr{S}_o}{dx}$.

The condition for the existence of a stagnation point at a given location is obtained by setting the derivative of the complex potential equal to zero at the appropriate location. Conformal transformations are used to give the complex potential and the resultant stagnation point condition a relatively simple form.

B. THE FLOW ABOUT SLENDER WINGS WITH VORTEX SEPARATION

The wing model considered here is a slender pointed wing with curved leading edges and arbitrary chordwise camber distribution. The wing is stipulated to be symmetrical about its longitudinal axis, which is aligned in the free stream direction (no yaw). The method discussed below is identical to that of Brown and Michael[3] for the case of the flat delta wing.

8

The governing equation is Laplace's equation in two dimensions

$$\phi_{\xi\xi} + \phi_{\eta\eta} = 0 \tag{10}$$

as previously discussed. The boundary conditions at the wing are that the normal velocities are zero and the flow separates tangentially at the edges. In the field, the boundary conditions are that the disturbances vanish at infinity. An additional condition is obtained by requiring each system of vortex and feeding sheet to be force free. The effect of camber is accounted for by allowing a chordwise varying cross flow velocity equal to $U_\infty \sin \alpha$ where α is the local angle of attack.

1. Solution

In obtaining a solution to Eq. (10), the complex velocity potential $\mathscr{F}(\mathscr{S},b)$ is introduced and is composed of the sum $\phi + i\psi$. Here $\mathscr{S}$ is the vector point coordinate, $\xi + i\eta$, (Fig. 3), b is the wing semi-span at a given X-station, and ψ is the stream function of the cross flow. The solution is obtained by conformal mapping of the cross flow past two symmetrically placed vortices of equal but opposite strength. Thus, in the θ-plane,

$$\mathscr{F}(\theta) = - \frac{i \Lambda_b}{2\pi} \log \frac{\theta - \theta_o}{\theta + \bar{\theta}_o} - i U_\infty \sin \alpha (\theta) \tag{11}$$

where θ_o is the vortex location and Λ_b is the vortex strength. Transforming Eq. (11) into the physical plane, in accordance with $\theta = \sqrt{\mathscr{S}^2 - b^2}$ yields

$$\mathscr{F}(\mathscr{S}) = - \frac{i \Lambda_b}{2\pi} \log \frac{\sqrt{\mathscr{S}^2 - b^2} - \sqrt{\mathscr{S}_o^2 - b^2}}{\sqrt{\mathscr{S}^2 - b^2} + \sqrt{\mathscr{S}_o^2 - b^2}} - i U_\infty \sin \alpha \sqrt{\mathscr{S}^2 - b^2} \tag{12}$$

The unknowns in the problem are the locations and strength of the concentrated vortices. These unknowns are determined through use of the boundary conditions. The following equation represents the condition that the vortex and feeding sheet be force-free (obtained from Eq. (9) by using Eq. (12) to give $w_{\mathscr{S}_o}$).

$$\left(\frac{1}{\Lambda_o} \frac{d\Lambda_o}{dx} + \frac{1}{b} \frac{db}{dx} + \frac{1}{\tan \alpha} \frac{d\alpha}{dx} \right) \left(\mathscr{S}_o - b \right) + \frac{d\mathscr{S}_o}{dx}$$

$$= i \tan \alpha \left\{ - b\Lambda_o \left[\frac{\bar{\mathscr{S}}_o}{(\bar{\mathscr{S}}_o - b^2)^{1/2} \left[(\bar{\mathscr{S}}^2 - b^2)^{1/2} + (\mathscr{S}_o^2 - b^2)^{1/2} \right]} + \frac{b^{2/3} \bar{\mathscr{S}}_o}{(\bar{\mathscr{S}}_o^2 - b^2)} \right] + \frac{\mathscr{S}_o}{(\mathscr{S}_o^2 - b^2)^{1/2}} \right\} \tag{13}$$

where $\mathscr{S}_o = b$ and $\Lambda_o = 2\pi U_\infty b\Lambda_o \sin \alpha$ where $b\Lambda_o = \frac{\bar{\theta}_o + \theta_o}{\theta_o \bar{\theta}_o}$. By requiring the existence of stagnation points on the wing leading edges, the following additional relation is obtained

$$\mathcal{L}_o = (2\pi U_\infty \sin\alpha) \frac{(\xi_o^2 - b^2)^{1/2} (\xi_o^2 - b^2)^{1/2}}{(\xi_o^2 - b^2)^{1/2} + (\xi_o^2 + b^2)^{1/2}} \qquad (14)$$

Equations (13) and (14) may be integrated to determine the position and strength of each separated vortex as functions of the longitudinal distance, X.

The evaluation of these relations is cumbersome and would have to be carried out by machine. However, approximate expressions for the vortex strength and location for the case of an uncambered delta wing are available[3]. The expressions are reproduced here with the note that a numerical evaluation of Eq. (15) will be necessary.

$$\frac{\alpha}{\epsilon} = \frac{4\eta_o}{b} \left[1 + \frac{1}{2} \left(\frac{\eta_o}{b}\right)^{2/3} \right] \qquad (15)$$

$$\frac{\xi_o - b}{b} = \frac{1}{2} \left(\frac{\eta_o}{b}\right)^{2/3} \left[1 - \frac{3}{4} \left(\frac{\eta_o}{b}\right)^{2/3} \right] \qquad (16)$$

$$\frac{\mathcal{L}_o}{2\pi b U_\infty \epsilon} = \frac{1}{2} \left[1 + \frac{3}{2} \left(\frac{\eta_o}{b}\right)^{2/3} \right] \frac{\alpha}{\epsilon} \qquad (17)$$

Here, ϵ represents the wing semi-vertex angle and ξ_o and η_o are the coordinate locations of the concentrated vortex.

2. Normal Force and Pressure Coefficient

The normal force acting on a wing ahead of a given X-station may be calculated through use of the following equation. This result is obtained by consideration of the downward momentum through a control volume enclosing the wing. Details of the derivation are given in Refs. 2 and 3.

$$N(x) = -\rho U_\infty \cos\alpha_o \iint \left[\phi_z - U_\infty \sin\alpha \right] dy \, dz \qquad (18)$$

Here α_o is the wing angle of attack and α is the local angle of attack. The area of integration is the entire ξ-η plane outside of the wing. Upon performing the required operations, the equation for the normal force becomes

$$N(x) = \rho_\infty U_\infty \cos\alpha_o \, \mathcal{L}_o R.P. \left(\frac{b^2}{2} (\xi_o^2 - b^2)^{1/2} \right)$$

$$+ \rho U_\infty^2 \cos\alpha_o \sin\alpha \, \pi b^2 \qquad (19)$$

10

The first term is the nonlinear contribution of the vortex separation while the remaining term is the slender-body theory result. The distribution of normal force along the wing may be found by differentiating $N(x)$.

The appropriate expression for the pressure coefficient is

$$C_p = \left(-\frac{2\phi_x}{U_\infty} + \alpha^2 - \frac{\phi_\xi^2}{U_\infty^2}\right)_{\eta=0} \qquad (20)$$

on the wing surface. The velocities, ϕ_x and ϕ_y, in the above equation are obtained from Eq. (12) through use of the following relations

$$\phi_x = R.P. \frac{\partial \bar{\phi}(\mathcal{S})}{\partial x} = \frac{\Gamma \xi}{2\pi}\left(\pm\pi + 2\tan^{-1}\frac{z_o - z}{y_o}\right) - \frac{\Gamma y_o \xi}{\pi}\frac{(b^2 - z^2)/z}{z^2 + 2z_o z + (y_o^2 + z_o^2)} + \frac{U_\infty \alpha b \xi}{z}$$

and

$$\phi_\xi = R.P. \frac{\partial \bar{\phi}(\mathcal{S})}{\partial \xi} = \left(\frac{\Gamma y_o}{\pi}\cdot\frac{1}{y_o^2 - (z_o - z)^2} - \alpha\right)\frac{\sqrt{b^2 - z^2}}{z} \qquad \begin{array}{c}(21)\\[1em](22)\end{array}$$

where the plus sign in Eq. (21) pertains to the leeward surface and the minus sign to the windward. The following transformations relate Eqs. (21) and (22) to the physical plane, $\mathcal{S} = \xi + i\eta$.

$$z = \pm\sqrt{b^2 - \xi^2}$$

$$y_o = \left\{\frac{-(b^2 + \eta_o^2 - \xi_o^2) + \left[(b^2 + \eta_o^2 - \xi_o^2)^2 + 4(\xi_o\eta_o)^2\right]^{\frac{1}{2}}}{2}\right\}^{\frac{1}{2}}$$

$$z_o = \left\{\frac{(b^2 + \eta_o^2 - \xi_o^2) + \left[(b^2 + \eta_o^2 - \xi_o^2)^2 + 4(\xi_o\eta_o)^2\right]^{\frac{1}{2}}}{2}\right\}^{\frac{1}{2}}$$

The plus-minus sign refers to the leeward and windward surface respectively.

3. Comparison with Experiment

The aerodynamic parameters selected for comparison are the lift coefficient, the bending moment about the root chord, and the semi-spanwise center of pressure. Since the nonlinear component of the aerodynamic characteristics is of primary interest, the linear component of the calculated results was determined by the experimental data around zero angle of attack. The calculated curves are, then, the sum of the experimental linear data plus the theoretical nonlinear results.

The data for several delta wings and an ogee wing are presented in the following figures. All data are presented versus wing angle of attack. The lift comparisons for the delta wing are presented in Figs. 9 thru 11 while the same for the ogee wing are given in Figs. 12 and 13. The calculations for the ogee wing do not include the effects of camber. It is noted that, in each case, theory overestimates the nonlinear forces. Much of the discrepancy may be attributed to the neglect of compressibility effects in the cross flow hypothesis. Also, the vortex core plus feeding sheet approximation will introduce some error, particularly in the vortex core location.

The bending moment and spanwise center of pressure comparisons are presented in Figs. 14 and 15 for a delta wing. Again it is seen that some discrepancy between theory and experiment is evident. Two factors will contribute to the divergence noted. One is that the predicted nonlinear forces are excessive. The second is that the vortex core location and hence its influence on the wing is further outboard than experiment[12] and more sophisticated theories[13, 14, 15] indicate. It may be noted, however,

11

that theory and experiment show an inboard trend in the center of pressure at the higher angles of attack.

C. THE FLOW ABOUT SLENDER BODIES WITH VORTEX SEPARATION

In this section, the considered model represents slender pointed bodies of elliptic cross-section and arbitrary camber distribution (Fig. 4). The restriction is made that the cross-sectional area variation in the streamline direction be non-negative (i.e. $dS/dx \geq 0$). The governing equation of motion is, as before (see pp. 7 and 8).

$$\phi_{\xi\xi} + \phi_{\eta\eta} = 0 \tag{23}$$

where ϕ is the velocity perturbation potential. The boundary conditions imposed on the problem are that the normal velocity at the surface be zero and the disturbances vanish at infinity. In addition, the previous conditions on the vortex system are required. The separation point on the body is obtained from experiment[1] or a satisfactory analytic procedure. The effect of camber is introduced by allowing a chordwise varying cross flow velocity equal to $U_\infty \sin \alpha$ where α is the local angle of attack. As in the case for wings, a more exact linear theory[5] should replace the slender body expression when applying the results of this discussion.

1. Solution

The complex potential, $\mathcal{P}(\mathcal{Y}) = \phi + i\psi$, is introduced in obtaining a solution to Eq. (23). ψ represents the cross flow stream function while $\mathcal{Y}$ represents the complex variable defined as $\mathcal{Y} = \xi + i\eta$. The general form of the solution is acquired through a conformal transformation of a flow field which contains the primary features of the physical problem. The approach taken here begins with the flow past a vertical line and vortex pair (Fig. 5). The resulting flow may be represented by

$$\mathcal{P}(\theta) = -\frac{i\Gamma_1}{2\pi} \log_e \frac{\theta - \theta_1}{\theta + \theta_1} - iU_\infty \sin \alpha (\theta) \tag{24}$$

where θ is the complex variable in the θ-plane $(\theta = y + iz)$, θ_1 is the location of the vortex $(\theta = y_1 + iz_1)$, and Γ_1 is the vortex strength. The transformation that will give the separated flow about an elliptical cross-section is

$$\theta = \frac{(k^2 - h^2)\mathcal{Y} + (k^2 + h^2)(\mathcal{Y} - 4k^2)^{1/2}}{2k^2} \tag{25}$$

Under this transformation, the potential function becomes

$$\bar{\phi}(\mathcal{I}) = -\frac{i\Gamma_1}{2\pi} \log \left\{ \frac{(\ell^2-h^2)(\mathcal{I}+\bar{\mathcal{I}}_1)+(\ell^2+h^2)\left[(\mathcal{I}^2-4\ell^2)^{1/2}+(\bar{\mathcal{I}}_1^2-4\ell^2)^{1/2}\right]}{(\ell^2-h^2)(\mathcal{I}-\mathcal{I}_1)+(\ell^2+h^2)\left[(\mathcal{I}^2-4\ell^2)^{1/2}-(\mathcal{I}_1^2-4\ell^2)^{1/2}\right]} \right\}$$

$$-i \sin\alpha \left[\frac{(\ell^2-h^2)\mathcal{I}+(\ell^2+h^2)(\mathcal{I}^2-4\ell^2)^{1/2}}{2\ell^2} \right] \tag{26}$$

where the vertical line has been transformed to an ellipse with horizontal semi-axis $b = \frac{h^2+\ell^2}{h}$ and vertical semi-axis $a = \frac{h^2-\ell^2}{h}$ (Fig. 5).

The unknowns in Eq. (26) are the strengths and locations of the vortices. Two conditions are required in order to specify these parameters. The first condition is that the vortex and its associated feeding sheet be force free. The second is that the flow field have cross flow stagnation points at given locations on the body (corresponding to empirically established separation lines).

The general expression for the force balance equation for this case may be written

$$U_\infty \frac{d\Gamma_1}{dx}(\mathcal{I}_1-\mathcal{I}_1') = \Gamma_1\left(V_{\mathcal{I}_1}^* - U_\infty \frac{d\mathcal{I}_1}{dx} + S_1\right) \tag{27}$$

where $V_{\mathcal{I}_1}^*$ is the cross flow velocity at $\mathcal{I}_1$ due to the potential $\bar{\phi}(\mathcal{I})$ minus the vortex at $\mathcal{I}_1$, and S_1 is the component due to the cross-sectional area variation. The expression for the velocity $V_{\mathcal{I}_1}^*$ at $\mathcal{I}_1$ may be written

$$V_{\mathcal{I}_1}^* = \frac{d}{d\mathcal{I}} \left\{ \bar{\phi}(\mathcal{I}) + \frac{i\Gamma_1}{2\pi} \log\left((\ell^2-h^2)(\mathcal{I}-\mathcal{I}_1')+(\ell^2+h^2)\left[(\mathcal{I}^2-4\ell^2)^{1/2} \right.\right.\right.$$
$$\left.\left.\left. - (\mathcal{I}_1^2-4\ell^2)^{1/2}\right]\right)\right\} \mathcal{I}=\mathcal{I}_1 \tag{28}$$

The velocity S_1 is obtained as follows. First the complex potential function for an axisymmetric source of strength A is specified

$$Q_s(\sigma) = A \ln(\sigma) \tag{29}$$

the transformation

$$\sigma = \frac{1}{2}\left[\mathcal{I} + \sqrt{\mathcal{I}^2-4\ell^2}\right] \tag{30}$$

maps the circle of radius h onto an ellipse of horizontal semi-axis $h + \frac{k^2}{h}$ and vertical semi-axis $h - k^2/h$. Hence the potential function may be written

$$Q_s \,(\mathcal{S}) = A \, log \left[\mathcal{S} + \sqrt{\mathcal{S}^2 - 4k^2} \right] \tag{31}$$

for which the velocity is found to be

$$\bar{\mathcal{S}}_1 = \frac{dQ_s}{d\mathcal{S}} = \frac{A}{\sqrt{\mathcal{S}^2 - 4k^2}} \tag{32}$$

the strength, A , of the source may be obtained through the following considerations.

The velocity due to the source must account for the rate of expansion of the ellipse. Consequently, the following expression holds at the point $\mathcal{S} = (h^2 + k^2/h)$:

$$\bar{S} \cdot U_\infty \cos \alpha \, \frac{db}{dx} = \frac{A}{h - k^2/h} \tag{33}$$

where $\frac{db}{dx}$ is the rate of expansion of the horizontal semi-axis of the body contour. Solving Eq. (33) for A and substituting into Eq. (32) gives the completed expression for S_1 :

$$S_1 = \frac{h - k^2/h}{\sqrt{\mathcal{S}^2 - 4k^2}} \, U_\infty \cos \alpha \, \frac{db}{dx} \tag{34}$$

Substituting Eqs. (28) and (34) into Eq. (27) gives the following result for the force balance equation.

$$\left(\frac{1}{\lambda_1} \frac{d\lambda_1}{dx} + \frac{1}{b} \frac{db}{dx} + \frac{1}{\tan\alpha} \frac{d\alpha}{dx} \right)\left(\mathcal{S}_1 - \mathcal{S}'_1 \right) + \frac{k^2 h^2}{h(\bar{\mathcal{S}}^2 - 4k^2)^{1/2}} \frac{db}{dx} + \frac{d\mathcal{S}_1}{dx} =$$

$$i \tan\alpha \left\{ -b\lambda_1 \left[\frac{k^2 h^2 + \mathcal{S}_1 \frac{k^2 + h^2}{(\mathcal{S}_1^2 - 4k^2)^{1/2}}}{(k^2 - h^2)(\mathcal{S}_1 + \mathcal{S}') + (k^2 + h^2)\left[(\mathcal{S}_1^2 - 4k^2)^{1/2} + (\mathcal{S}^2 - 4k^2)^{1/2} \right]} \right. \right.$$

$$+ \frac{2l^2(l^2+h^2)}{(l^2+h^2)(\bar{\varsigma}_1^2 - 4l^2)^{1/2} + \bar{\varsigma}_1(l^2+h^2)(\bar{\varsigma}_1^2 - 4l^2)}$$

$$+ \frac{1}{2l^2}\left[l^2 + h^2 + \bar{\varsigma}_1 \frac{l^2+h^2}{(\bar{\varsigma}_1^2 - 4l^2)^{1/2}}\right]\Bigg\} \tag{35}$$

where the vorticity has been normalized by the horizontal semi-axis, $\Gamma = 2\pi b \lambda V_\infty \sin\alpha$.

The condition for a stagnation point of the cross flow at the point ς_1' requires that

$$\bar{\omega}_1' = \frac{dQ}{d\varsigma}\bigg|_{\varsigma = \varsigma_1'} = 0 \tag{36}$$

Upon carrying out the above operation, the additional relation is obtained:

$$b\lambda_1 = \frac{1}{2l^2}\left[(h^2+l^2)\left[(\varsigma_1'^2 - 4l^2)^{1/2} + (\varsigma_1^2 - 4l^2)^{1/2}\right] - (h^2 - l^2)(\varsigma_1' + \bar{\varsigma}_1)\right] \times$$

$$\times \left[(h^2+l^2)\left[(\varsigma_1'^2 - 4l^2)^{1/2} - (\varsigma_1^2 - 4l^2)^{1/2}\right] - (h^2 - l^2)(\varsigma_1' - \varsigma_1)\right] \Bigg/ \Bigg\{ (h^2 - l^2)(\varsigma_1' \cdot \bar{\varsigma}_1)$$

$$- (h^2 + l^2)\left[(\varsigma_1'^2 - 4l^2)^{1/2} + (\bar{\varsigma}_1^2 - 4l^2)^{1/2}\right]\Bigg\} \tag{37}$$

Equations (35) and (37) are derived from the solution of Eq. (23) and the corresponding boundary conditions. As previously discussed, it is necessary to prescribe the location of flow separation, ς_1' . The solution of the equations will probably require a machine computation.

2. Normal Force and Pressure Coefficient

The normal force acting on the portion of a body ahead of a given X -station may be obtained from the following equation.

$$N(X) = -\rho \varsigma V_\infty \cos\alpha_0 \iint \left[\phi_\eta - V_\infty \sin\alpha\right] d\xi\, d\eta \tag{38}$$

where α_0 is the body angle of attack. Evaluation of the above equation results in the following expression

$$N(X) = \rho V_\infty \cos\alpha_0 \, \mathcal{LRP.}\left[\frac{h^2 + l^2}{l^2}(\theta_1^2 - 4l^2)^{1/2} - \frac{(h^2 - l^2)}{l^2}\theta_1\right] + \rho V_\infty^2 \cos\alpha_0 \sin\alpha \pi\left(h + \frac{l^2}{h}\right)^2 \tag{39}$$

15

where

$$\theta_l = \frac{(t^2-h^2)\mathcal{J}_l + (t^2+h^2)(\mathcal{J}_l^2 - 4t^2)^{1/2}}{2t^2} \tag{40}$$

the distribution of normal force along the body may be found by differentiating $N(x)$.

The appropriate expression for the pressure coefficient is

$$C_p = -\frac{2\phi_\chi}{U_\infty} + \alpha^2 - \frac{(\phi_\xi^2 + \phi_\eta^2)}{U_\infty^2} \tag{41}$$

The velocities, ϕ_χ, ϕ_y, and ϕ_z, may be obtained from Eq. (26) through use of the following definitions.

$$\phi_\chi = R.P. \left\{ \frac{\partial \overline{\phi}(y)}{\partial x} \right\}$$

$$\phi_\xi = R.P. \left\{ \frac{d\overline{\phi}}{d\mathcal{S}} \right\} \tag{42}$$

and

$$\phi_\eta = -I.P. \left\{ \frac{d\overline{\phi}}{d\mathcal{S}} \right\} \tag{43}$$

3. Comparison with Experiment

The parameters selected for comparison purposes are the normal force, pitching moment and normal force distribution. As in the previous sections, the linear component of the calculated curve was obtained from experiment except for the force distribution where part of the linear distribution was obtained from hybrid theory. The theoretical curves show results based on the assumption of laminar boundary layer separation and of turbulent separation. Although the comparisons indicate the prevalence of laminar flow, the turbulent flow case is shown in order to demonstrate the importance of selecting the correct boundary layer type in calculations.

The configuration tested was an ogive-cylinder and is shown to scale in the force distribution figures. The free-stream Mach number was 1.98 with Reynolds numbers of 0.439×10^6 and 0.146×10^6 based on the cylinder diameter. The normal force comparison is represented in Fig.16. The agreement between experiment and the laminar curve is seen to be very good. The pitching moment comparison in Fig.17 also indicates good agreement although some divergence is noted at the higher angles of

16

attack. The normal force distribution comparisons shown in Figs. 18a thru 18d show approximate agreement at the lower angles of attack and significant discrepancy at the higher angles of attack. Part of the discrepancy may be due to limitations of the hybrid theory. It is seen, however, that stream-wise trends in the experimental and theoretical curves do show some correspondence.

D. THE FLOW ABOUT WING-BODY COMBINATIONS WITH VORTEX SEPARATION

The separation flow mechanics about slender wing-body combinations are considered in this section. Each component (wing or body) of the configuration will have a corresponding vortex system as in the previous models; the condition for determining the vortex strengths and locations, however, will be different in the interaction regions of the model. This factor is discussed below.

The geometry of the wing-body configurations consists of a simple joining together of the separate wing and body models previously discussed (Fig. 6). An important restriction is that the model be laterally and vertically symmetrical (i.e., a body cross-section primary axis be in the wing plane).

The governing equation is Laplace's equation in two dimensions as in the previous sections. The usual boundary conditions on Eq. (8) are applied; there is no flow through the surfaces and perturbations vanish at infinity. The condition of continuous pressure in the flow field (violated by the vortex sheet in the vortex model) is relaxed by requiring the vortex core plus feeding sheet to be force free.

In order to obtain the nonlinear lift load, the strengths and locations of the vortex cores (wing and body) everywhere along the configurations must be determined. For the wing and body alone, the location of the separation stagnation point plus the force-free vortex system were directly applied to determine the vortex characteristics. For wing-body combinations, however, interaction increases the difficulty of the problem; in particular, the aerodynamic interaction precludes our locating the body separation point – if it exists at all. The approach taken here is to neglect body separation mechanics in the cross-flow region of the wing, i.e., the body vortex may change location but not strength (see Ref. 2).

It is seen that three cross-flow regions can exist. The first region will be that portion of the body ahead of the wing while the second, as discussed above, constitutes the wing-body interaction region. The third region concerns the portion of the body that may be behind the wing trailing edge. The vortex model conditions in each region may be stated as follows (see Fig. (7)):

Region I: 1) The vortex core plus feeding sheet is force-free.
             2) Flow separation is stipulated to occur at some location (obtained by experiment or an acceptable theory).

Region II: 1) The wing vortex core plus feeding sheet is force-free; the body vortex core alone is force free (no feeding sheet).

2) Separation is stipulated to exist at the wing edges with no separation from the body.

Region III: 1) The body vortex core plus feeding-sheet is force-free; the trailing wing vortex cores are force-free.
2) Separation exists at some given location on the body.

As will be seen from the subsequent discussion, the problem, as formulated above, is extremely formidable; for this reason, an abbreviated flow model, which retains the basic features, is also presented. This model will be discussed following the development of the more accurate model outlined above.

1. Solution

a. "Primary" Model

A typical slender wing-body configuration will generally consist of the three distinct regions just defined. These regions are indicated and designated in Fig. (7). Each of these regions is separately discussed below.

(a) Region I

Slender body theory holds that axial velocity perturbations are much smaller than lateral perturbations. Hence, except for separation-induced circulation which is convected downstream, there is no interaction between chordwise stations. In particular, the portion of the body ahead of the wing may be analyzed as though the wing did not exist. The procedure for analyzing the aerodynamics in this region is therefore identical to that of Section III-C.

(b) Region II

The general solution to the cross flow in this region is found through conformal transformations of some simple flow model as in the previous sections. The first step is to map the flow about two pairs of symmetrically placed vortices as shown in Fig. (8a). The complex potential function may be written

$$\phi(\theta) = \frac{i\Gamma_o}{2\pi} \ln\left(\frac{\theta-\theta_o}{\theta+\bar{\theta}_o}\right) - \frac{i\Gamma_1}{2\pi} \ln\left(\frac{\theta-\theta_1}{\theta+\bar{\theta}_1}\right) - i U_\infty \alpha \theta \qquad (44)$$

Applying the transformation $\theta = \sqrt{\sigma^2 - s'^2}$ to the above equation results in the cross flow shown in Fig. (8b) and transforms the segment of the imaginary axis from $-s'$ to $+s'$ to a horizontal line segment. The complex potential becomes

$$\phi = -\frac{i\Gamma_o}{2\pi} \ln\left(\frac{\sqrt{\sigma^2-s'^2}-\sqrt{\sigma_o^2-s'^2}}{\sqrt{\sigma^2-s'^2}+\sqrt{\sigma_o^2-s'^2}}\right) + \frac{i\Gamma_1}{2\pi} \ln\left(\frac{\sqrt{\sigma^2-s'^2}-\sqrt{\sigma_1^2-s'^2}}{\sqrt{\sigma^2-s'^2}+\sqrt{\sigma_1^2-s'^2}}\right) - i U_\infty \alpha \sqrt{\sigma^2-s'^2} \qquad (45)$$

18

One additional transformation gives the required cross flow

$$\sigma = \left\{ (R^2 - r^2) \, \mathcal{I} + (k^2 + r^2)(\mathcal{I}^2 - 4k^2)^{1/2} \right\} / 2k^2 \tag{46}$$

where $R_2^2 (a+b)(a-b)/4$ and $r = (a+b)/2$. The resulting function represents the flow about an elliptical two dimensional body with a mid-plane wing and four vortex systems (Fig. 8c). The potential function may be written as shown on the following page.

19

$$\phi(Y) = -\frac{i\Omega}{2\pi} \ln \left[\frac{\sqrt{\frac{(L^2-r^2)^2 \bar{\mathcal{J}}_y^2 + 2(L^6-r^6)\bar{\mathcal{J}}_y(\bar{\mathcal{J}}_y^2-4L^2)^{1/2} + (L^2+r^2)^2(\bar{\mathcal{J}}_y^2-4L^2)}{4L^2} - S'^2}}{\sqrt{\frac{(L^2-r^2)^2 \bar{\mathcal{J}}_y^2 + 2(L^6-r^6)\bar{\mathcal{J}}_y(\bar{\mathcal{J}}_y^2-4L^2)^{1/2} + (L^2+r^2)^2(\bar{\mathcal{J}}_y^2-4L^2)}{4L^2} - S'^2}} \right]$$

$$+ \frac{i\Omega}{2\pi} \ln \left[\frac{\sqrt{\frac{(L^2-r^2)^2 \bar{\mathcal{J}}_y^2 + 2(L^6-r^6)\bar{\mathcal{J}}_y(\bar{\mathcal{J}}_y^2-4L^2)^{1/2} + (L^2+r^2)^2(\bar{\mathcal{J}}_y^2-4L^2)}{4L^2} - S'^2}}{\sqrt{\frac{(L^2-r^2)^2 \bar{\mathcal{J}}_y^2 + 2(L^2-r^2)\bar{\mathcal{J}}_y(\bar{\mathcal{J}}_y^2-4L^2)^{1/2} + (L^2+r^2)^2(\bar{\mathcal{J}}_y^2-4L^2)}{4L^2} - S'^2}} \right]$$

$$- i U\alpha \sqrt{\frac{(L^2-r^2)^2 \bar{\mathcal{J}}_y^2 + 2(L^4+r^4)\bar{\mathcal{J}}_y(\bar{\mathcal{J}}_y^2-4L^2)^{1/2} + (L^2+r^2)^2(\bar{\mathcal{J}}_y^2-4L^2)}{4L^2} - S'^2}$$

$$\tag{47}$$

This function represents the flow about a two-dimensional wing-body combination. In order to take account of the growth of the body in the X-direction, the complex velocity potential of a source within the body must be added. The strength of the source must be such that the outflow at the surface of the body just matches the growth rate of the body.

The complex velocity of the source for an elliptic cross-section is found by transforming the potential for a circular body. The complex velocity potential for the source representing the rate of change of a circular cross-section may be written (Section III-C-1)

$$\phi_s(X) = U_\infty \, r \frac{dr}{dX} \ln X \tag{48}$$

where $X = y + i z$. Now, the circle in the X-plane may be transformed to an ellipse in the $\mathcal{Y}$-plane by the transformation

$$X = \frac{1}{2}\left(\mathcal{Y} + \sqrt{\mathcal{Y}^2 - 4 k^2} \right) \tag{49}$$

The potential due to the source in the $\mathcal{Y}$-plane becomes

$$\phi_s(\mathcal{Y}) = U_\infty \, r \frac{dr}{dX} \ln\left(\frac{1}{2}\mathcal{Y} + \frac{1}{2}\sqrt{\mathcal{Y}^2 - 4 k^2} \right) \tag{50}$$

The complex potential for treating the three-dimensional wing-body combination by slender body techniques is thus

$$\phi_{3-0}(\mathcal{Y}) = \phi(\mathcal{Y}) + \phi_s(\mathcal{Y}) \tag{51}$$

where $\phi(\mathcal{Y})$ is given by Eq. (47).

The unknowns in this region of the configuration are the strength and location of the wing vortices and the location of the body vortices, the strength being a constant and equal to that at the beginning of the region. It is seen necessary that three conditions be imposed on the problem to allow solution. These conditions are that (1) a stagnation point exist at the wing leading edge (flow separation), (2) the wing vortex core plus feeding sheet be force free, and (3) the body vortex core <u>alone</u> be force free. The last condition dictates that the vortex core follow a streamline of the three-dimensional flow pattern. The mathematical formulation of each of these conditions is described below.

The first condition may be found by requiring a stagnation point at the origin of the θ-plane since the wing tip location maps to the origin when the transformations are applied. The flow in the θ-plane is represented by

$$\phi(\theta)_{(3-0)} = -\frac{i \Gamma_0}{2\pi} \ln\left(\frac{\theta - \theta_0}{\theta + \bar{\theta}_0}\right) - \frac{i \Gamma_1}{2\pi} \ln\left(\frac{\theta - \theta_1}{\theta + \bar{\theta}_1}\right) - i\, U_\alpha \theta + \phi_s(\theta) \tag{52}$$

21

where $\phi_s(\theta)$ is the transformed complex velocity potential of the source and is given by

$$\phi_s = U_\infty \, r \, \frac{dr}{dx} \, \ln\left(\frac{1}{2}\, \mathcal{Y} + \frac{1}{2}\, \sqrt{\mathcal{Y}^2 - 4\ell^2}\right) \tag{53}$$

where

$$\mathcal{Y} = \frac{(\ell^2 + r^2)\left(\sqrt{\theta^2 + s'^2 + 4r^2}\right) - (\ell^2 - r^2)\left(\sqrt{\theta^2 + s'^2}\right)}{2r^2} \tag{54}$$

which may be found from the inverse of the transformations $\sigma = \sigma(\mathcal{Y})$ and $\theta = \theta(\sigma)$ given above. In the present discussion, ϕ instead of $\phi_{(3-D)}$ will denote the total complex potential.

Taking the derivative with respect to θ :

$$\frac{d\phi(\theta)}{d\theta} = -\frac{i\Gamma_0}{2\pi}\left(\frac{\theta + \bar{\theta}_0}{\theta - \theta_0}\right)\left(\frac{\theta_0 + \bar{\theta}_0}{(\theta + \bar{\theta}_0)^2}\right) - \frac{i\Gamma_1}{2\pi}\left(\frac{\theta + \bar{\theta}_1}{\theta - \theta_1}\right)\left(\frac{\theta_1 + \bar{\theta}_1}{(\theta + \theta_1)^2}\right) - i U_\infty \alpha + \frac{d\phi_s(\theta)}{d\theta} \tag{55}$$

Requiring a stagnation point at the origin dictates that

$$\frac{d\phi(\theta)}{d\theta}\bigg|_{\theta = 0} = 0 \tag{56}$$

Consequently, the following expression results

$$\frac{\Gamma_0}{2\pi}\left(\frac{1}{\theta_0} + \frac{1}{\bar{\theta}_0}\right) + \frac{\Gamma_1}{2\pi}\left(\frac{1}{\theta_1} + \frac{1}{\bar{\theta}_1}\right) = U_\infty \alpha \tag{57}$$

The second condition (force condition on wing vortices) may be directly represented by Eq. (9) of Section III-A.

$$U_\infty \frac{d\Gamma}{dx}\left(\mathcal{Y}_0 - \mathcal{Y}_0'\right) - V_{\mathcal{Y}_0}^* \, \Gamma_0 = 0 \tag{58}$$

where

$$V_{\mathcal{Y}_0}^* = \left(\frac{d\phi}{d\mathcal{Y}}\right)_{\mathcal{Y} = \mathcal{Y}_0} - U \frac{d\mathcal{Y}_0}{dx}$$

The expression for $(d\phi/d\mathcal{Y})_{\mathcal{Y} = \mathcal{Y}_0}$ may be obtained by subtracting the contribution due to $\Gamma_{\mathcal{Y} = \mathcal{Y}_0}$ from ϕ and then performing the differentiation. Considering the θ -plane, the required expression for the potential may be written

$$\phi(\theta) = -\frac{i\Gamma_0}{2\pi}\ln\left(\frac{\theta - \theta_0}{\theta + \bar{\theta}_0}\right) - \frac{i\Gamma_1}{2\pi}\ln\left(\frac{\theta - \theta_1}{\theta + \bar{\theta}_1}\right) - i U_\infty \alpha\, \theta + \phi_s(\theta) + \frac{i\Gamma_0}{2\pi}\ln(\theta - \theta_0) \tag{59}$$

Differentiating with respect to θ and evaluating at θ_0 gives

$$\frac{d\bar{\phi}(\theta)}{d\theta}\bigg|_{\theta=\theta_0} = \frac{i\Gamma_0}{2\pi}\left(\frac{1}{\theta_0 + \bar{\theta}_0}\right) - \frac{i\Gamma_1}{2\pi}\frac{\bar{\theta}_1 + \theta_1}{(\theta_0 - \theta_1)(\theta_0 + \bar{\theta}_1)} - i U_\infty \alpha + \frac{d\bar{\phi}_s(\theta)}{d\theta}\bigg|_{\theta=\theta_0}$$

(60)

where

$$\frac{d\bar{\phi}_s}{d\theta} = \frac{d\bar{\phi}_s}{d\mathcal{G}}\frac{d\mathcal{G}}{d\theta}$$

(61)

$$= U_\infty \, r \frac{dr}{dx}\left(\frac{1}{\mathcal{G}+\sqrt{\mathcal{G}^2 - 4t^2}}\right)\left(1 + \frac{\mathcal{G}}{\sqrt{\mathcal{G}^2 - 4t^2}}\right)\frac{d\mathcal{G}}{d\theta}\bigg|_{\theta=\theta_0}$$

and

$$\frac{d\mathcal{G}}{d\theta} = \left(\frac{t^2 + r^2}{2r^2}\right)\left(\frac{\theta}{\sqrt{\theta^2 + S'^2 + 4r^2}}\right) - \left(\frac{t^2 - r^2}{2r^2}\right)\left(\frac{\theta}{\sqrt{\theta^2 + S'^2}}\right)$$

(62)

The final condition of the force free body vortex is obtained by simply requiring the vortex core to follow a streamline, i.e., the velocity perpendicular to the vortex must be zero. Consequently, we may write $V_{\mathcal{G}_1}^* = 0$ or

$$\left(\frac{d\bar{\phi}}{d\mathcal{G}}\right)_{\mathcal{G}=\mathcal{G}_1} - U_\infty \frac{d\mathcal{G}_1}{dx} = 0$$

(63)

The system of three simultaneous equations to be solved for the three unknowns Γ_0, $\mathcal{G}_0$, $\mathcal{G}_1$ (Γ_1 is assumed constant) may be written as:

(64)

$$\frac{\Gamma_0}{2\pi}\left(\frac{1}{\theta_0} + \frac{1}{\bar{\theta}_0}\right) + \frac{\Gamma_1}{2\pi}\left(\frac{1}{\theta_1} + \frac{1}{\bar{\theta}_1}\right) = U\alpha$$

$$\frac{d\Gamma_0}{dx} - \frac{V_{\mathcal{G}_0}^*}{U}\left(\frac{1}{\mathcal{G}_0 - \mathcal{G}}\right)\Gamma_0 = 0$$

(65)

$$V_{\mathcal{G}_1}^* = 0$$

(66)

It is obvious that solution of the above set of equations must be accomplished numerically, in order to obtain meaningful solutions with a reasonable amount of effort. Such a solution would be in the form of a simultaneous numerical integration in the X-direction of the force equations, (65) and (66) subject to the "boundary condition" (64). The solution may then be started at any axial station X, provided the initial

values of $\mathcal{L}_0$, $\mathcal{L}_1$, $\mathcal{S}$ and $\mathcal{S}_i$ are known. The body cross section, given by a and b, and the total span s must be prescribed explicitly as functions of x.

(c) Region III

This region of the wing-body configuration consists of the aft body segment and the body and wing vortex systems. The unknowns are the location of the wing and body vortex cores and the strength of the body vortex, the wing vortex strength remaining constant. It is seen that the problem is very similar to that of Region II. The corresponding equations may be written as follows:

$$-\frac{\mathcal{L}_0}{2\pi}\frac{\bar{\theta}_0+\theta_0}{(\theta_1'-\theta_0)(\theta_1'+\bar{\theta}_0)} - \frac{\mathcal{L}_1}{2\pi}\frac{\bar{\theta}_1+\theta_1}{(\theta_1'-\theta_1)(\theta_1'+\bar{\theta}_1)} + \frac{d\bar{\phi}_s}{d\theta}\bigg|_{\theta=\theta_1'} = U_\infty\alpha \tag{67}$$

$$\frac{d\mathcal{L}}{dx} - \frac{v_{\mathcal{S}_1}^*}{U}\left(\frac{1}{\mathcal{S}_1-\mathcal{S}_1'}\right)\mathcal{L}_1 = 0 \tag{68}$$

$$v_{\mathcal{S}_0}^* - \left(\frac{d\bar{\mathcal{L}}_1}{d\mathcal{S}}\right)_{\mathcal{S}=\mathcal{S}_0} - U_\infty\frac{d\mathcal{S}_0}{dx} = 0 \tag{69}$$

Equation (67) requires a stagnation point on the body at $\theta = \theta_1'$, Eq. (68) stipulates a force-free body vortex-feeding sheet system, and the third equation requires a force-free wing vortex. Again, the solution to the problem will require a machine computation involving the procedure of Region II.

b. Approximate Model

As was the case for the "primary" model discussed in the preceding paragraphs, the approximate model will comprise three regions (Fig. (7)). Each of these regions is discussed in turn.

(a) Region I

The approximate and primary models are identical in this region hence, the results of Section III-C may be directly applied.

(b) Region II

The general solution in this region is the same as for the primary model; the basic differences enter through specification of the body and wing vortex characteristics (strength and location). In this approximate model, the body vortex location, normalized to the local body dimension, does not vary with x. Also, the wing vortex mechanics are assumed to be subject to the flow associated with the wing alone, i.e., the body and its vortex pair have no influence. Consequently, the body vortex (with no feeding sheet) follows a trajectory dictated by body geometry in the region. The wing vortex has a distribution of strength and position identical with the wing alone case (Section III-B).

24

(c) Region III

The simplifying assumptions applied to the vortex mechanics of Region II also apply in this region consisting of the body and its vortex system along with the trailing vortex cores of the wing. The wing vortex cores strengths and positions are assumed constant and the vortex mechanics of the body are identical to those of Section III-C with no effect of the wing vortex cores.

2. Normal Force and Pressure Coefficient

Once the strengths and positions of the separated vortices are found, the resulting lift distributions on the wing and body may be determined. The total normal force up to station X is equal to the rate of downward momentum emerging from the $\mathcal{S}$-plane

$$N(x) = -\rho U_\infty \cos \alpha \iint_{A(x)} \left[V_\eta - U_\infty \sin \alpha \right] d\xi d\eta \tag{70}$$

where $A(x)$ is the area of the $\mathcal{S}$-plane outside the wing-body combination. Transforming to the θ-plane and integrating (see Ref. 2) gives the following result for the normal force

$$N(x) = \rho U_\infty \cos \alpha \ R.P. \left[\mathcal{L}_0 (\theta_0 + \bar{\theta}_0) + \mathcal{L}_1 (\theta_1 + \bar{\theta}_1) \right]$$

$$+ \rho U_\infty^2 \sin \alpha \cos \alpha \left(r - \frac{k^2}{r} \right)\left(r + \frac{k^2}{r} \right) \pi$$

$$+ \rho U_\infty^2 \sin \alpha \cos \alpha \left\{ \left(\frac{k^2 + r^2}{2r^2} \right)(s'^2 + 4r^2)\pi - \left(\frac{k^2 r^2}{2r^2} \right) s'^2 \pi \right\} \tag{71}$$

The axial normal force distribution may be obtained by differentiating Eq. (71).

The expression for the pressure coefficient may be written

$$C_p = -\frac{2\phi_x}{U_\infty} + \alpha^2 - \frac{(\phi_\xi^2 + \phi_\eta^2)}{U_\infty^2} \tag{72}$$

25

where, as in the foregoing discussions, the perturbation velocities are
defined as

$$\phi_x = R.P. \left\{ \frac{\partial \bar{\phi}(y)}{\partial x} \right\} \tag{73}$$

$$\phi_\xi = R.P. \left\{ \frac{d\bar{\phi}(y)}{dy} \right\} \tag{74}$$

and

$$\phi_\eta = - I.P. \left\{ \frac{d\bar{\phi}(y)}{dy} \right\} \tag{75}$$

The pressure coefficient is difficult to evaluate analytically and a numerical
approach should be used. Computations of nonlinear lifting loads on
specific wing-body combinations are presented below. Corresponding
pressure distributions have not been computed.

3. Comparison with Experiment

The aerodynamic characteristics selected for comparison are
the lift and the pitching moment coefficients. As was the case for the
previous configurations, the theoretical nonlinear component was com-
bined with the experimental linear component to obtain the calculated
curve.

Data on a delta wing with an ogive-cylinder body was obtained for
comparison with theory[16]. The test of interest was made at a Mach
number of 1.50. The lift comparison is presented in Fig. 19 and the
comparison of the pitching moment results is in Fig. 20. Overestima-
tion of the nonlinear component of the force and moment coefficients
is apparent in the comparisons. Previous comparisons with the wing
and body alone indicate that the wing is primarily responsible. The
neglect of compressibility effects and the approximate vortex sheet
model are factors in the discrepancies.

SECTION IV

CONCLUSION

This report has been concerned with presenting methods for the analysis of the aerodynamics and static aeroelasity of slender configurations with vortex separation. The primary emphasis has been on the nonlinear aspect of the mechanics involved. Three configurations have been considered in the report: wings alone, bodies alone and wing-body combinations, each being investigated using the concepts of slender body theory to calculate nonlinear forces. Experimental comparisons for evaluating the theoretical results have also been presented.

Experimental comparisons with theory were designed to evaluate the theoretical nonlinear component of the aerodynamic characteristics considered. The linear components of the calculated curves were obtained from the experimental data around zero angle of attack. The theoretical nonlinear component was then added to the experimental linear component for comparison with the data. Results show that theory overestimates experiment on wing forces but is in good agreement on body forces. The neglect of compressibility effects in the cross-flow plane is apparently significant for the flow about wings. The separated vortex model of a vortex pair with feeding sheets of infinitesimal strength is also responsible.

While the two-vortex slender body model correctly predicts the trends of nonlinear forces, its quantitative limitations are apparent. The theory might be improved in two ways. One would be to account for compressibility effects, the other would use a more elaborate vortex model, such as multiple vortices or a continuous sheet rolling up on itself. In either case, the mathematical simplicity of the present theory would be lost; hence a considerable improvement in force prediction would be necessary to justify a lengthy complex calculation.

REFERENCES

1. Schindel, L. H., Effect of Vortex Separation on Lifting Bodies of Elliptic Cross Section, Aerophysics Laboratory, Mass. Inst. of Tech. Technical Report 118, 1965.

2. Borland, C.J., Methods of Calculating Aerodynamic Loads on Aircraft Structures: Part I - Wing-Body Interference Effects, Air Force Flight Dynamics Laboratory Technical Report 66-37, January, 1966.

3. Brown, C.E. and Michael, W.H., Jr., On the Slender Delta Wings with Leading Edge Separation, NACA TN 3430, 1955.

4. Bryson, A.E., Jr.,"Symmetric Vortex Separation on Circular Cylinders and Cones", Journal of Applied Mechanics, Vol. 26, No. 4, 1959.

5. Schindel, L. H., An Evaluation of Procedures for Calculating Aerodynamic Loads, Aerophysics Laboratory, Mass. Inst. of Tech. Technical Report 103, 1965.

6. Adams, M. C., "Leading-Edge Separation from Delta Wings at Supersonic Speeds", Journ. Aero. Sci. 20, 1953, p. 430.

7. Legendre, R., "Écoulement au voisinage de la pointe avant d'une aile à forte flèche aux incidences moyennes", La Recherche Aéronautique (ONERA), No. 31, 1953.

8. Edwards, R.H., "Leading Edge Separation from Slender Delta Wings", Journ Aero. Sci. 21, 1954, pp. 134-135.

9. Bartlett, G.E. and Vidal, R.J., Experimental Investigation of the Influence of Edge Shape on the Aerodynamic Characteristics of Low Aspect Ratio Wings at Low Speeds, Journal of the Aeronautical Sciences, Vol. 22, No. 8, August 1955.

10. Tosti, L. P., Low Speed Static Stability and Damping-in-Roll-Characteristics of Some Swept and Unswept Low-Aspect-Ratio-Wings, NACA TN 1468, 1947.

11. Isaacs, D., Measurements of Subsonic and Supersonic Speeds of the Longitudinal and Lateral Stability of a Slender Cambered Ogee Wing Including the Effects of a Fin, Canopy Nose and Trailing Edge Controls, ARC R and M No. 3390, 1965.

12.   Kaattari, G.E., Pressure Distributions on Triangular and Rectangular Wings to High Angles of Attack - Mach Numbers 1.45 and 1.97, NACA RM A54D19, 1954.

13.   Smith, J.H.B., "The Improved Calculation of the Mangler-Smith Model of Leading-Edge Separation from a Slender Delta Wing at Incidence", Presented at IUTAM Symposium on Concentrated Vortex Motions in Fluids, Ann Arbor, Mich., July 1964.

14.   Mangler, K.W., and Smith, J.H.B., Calculation of the Flow Past Slender Delta Wings with Leading-Edge Separation, R.A.E. TN. Aero. No. 2442 (See also Proc. Roy. Soc. A251, 1959, pp. 200-217).

15.   Perkins, E.W., and Jorgensen, L.H., Comparison of Experimental and Theoretical Normal-Force Distributions (Including Reynolds Number Effects) on an Ogive Cylinder Body at Mach Number 1.98, NACA TN 3716, 1956.

16.   Nielsen, J.N., Katzen, E.D., and Tang, K.K., Lift and Pitching Moment Interference Between a Pointed Cylindrical Body and Triangular Wings of Various Aspect Ratios at Mach Numbers of 1.50 and 2.02, NACA TN 3795, 1956.
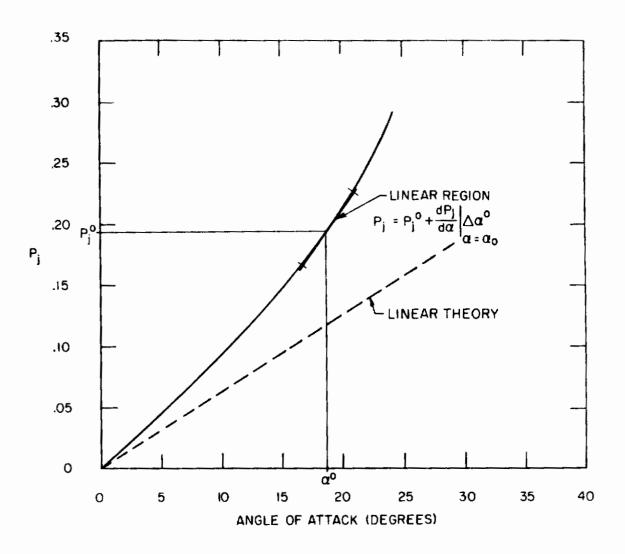
Figure 1. Example Plot of Pressure Versus Angle of Attack
Showing Linearization Technique

31
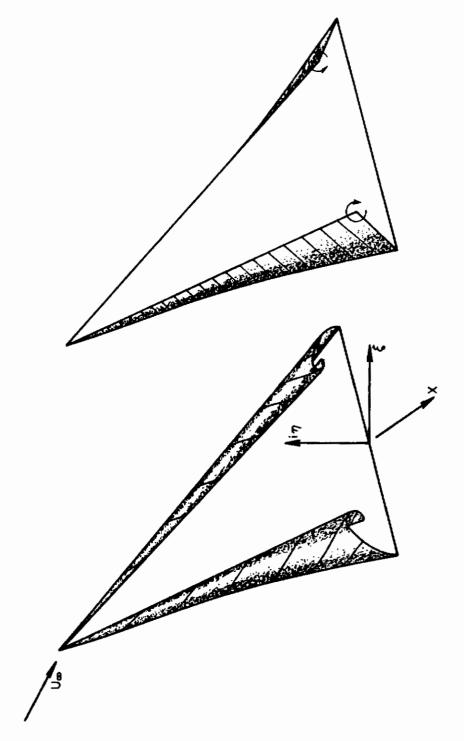
Figure 2. Schematic Drawings of Separated Flow Over a Slender Wing
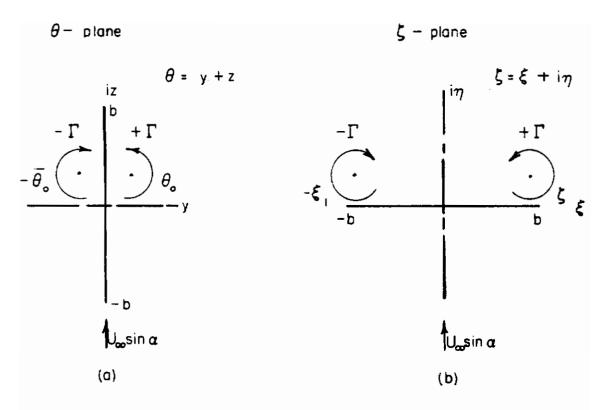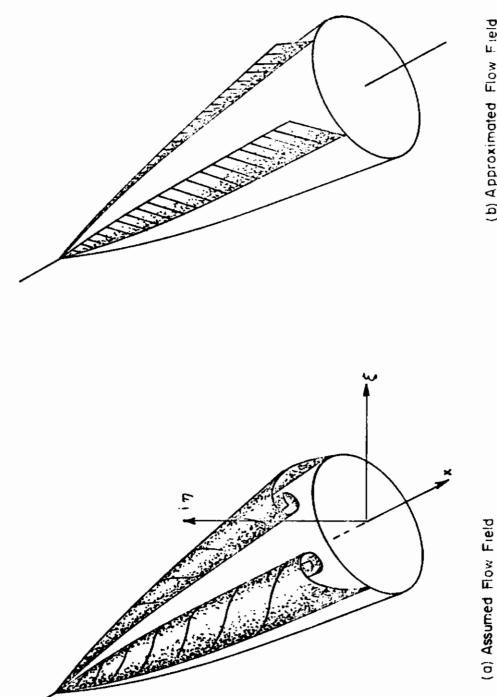
Figure 3. The Flow Past a Vertical Line and a Horizontal Line with a Symmetrical Set of Vortices

(b) Approximated Flow Field

(a) Assumed Flow Field

Figure 4. Schematic Drawings of Separated Flow Over a Slender Body

34
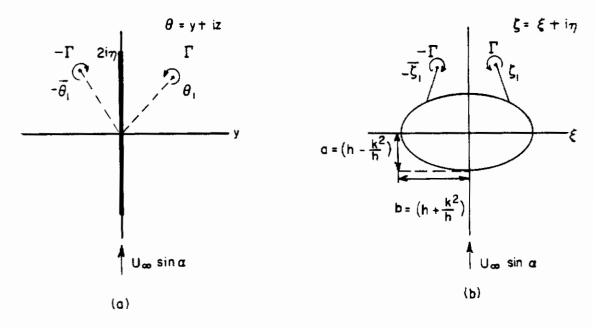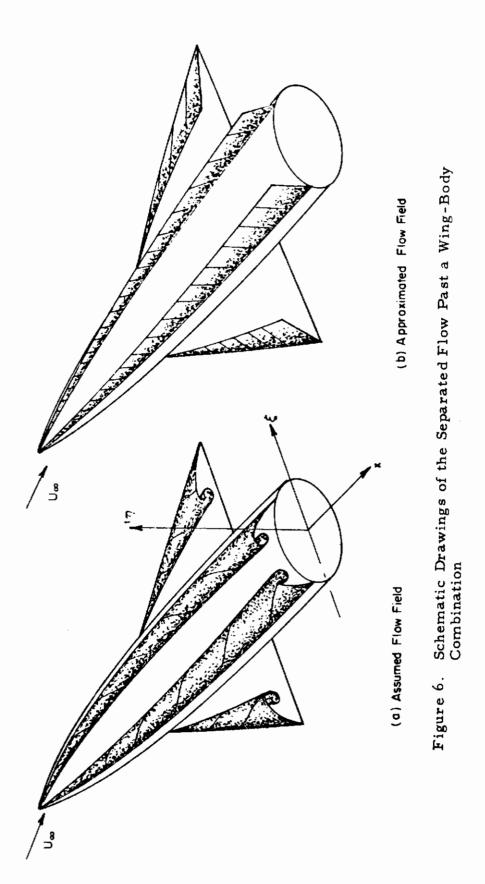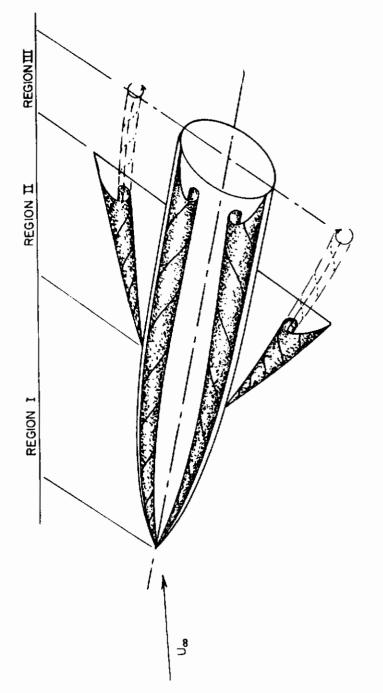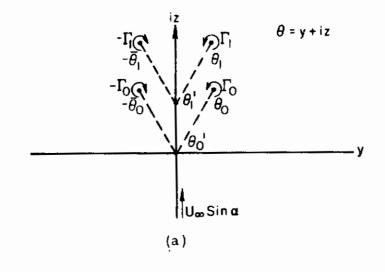
Figure 5. The Flow Past a Vertical Line, (a), and an Ellipse, (b), with a Symmetrical Set of Vortices

(b) Approximated Flow Field

(a) Assumed Flow Field

Figure 6.   Schematic Drawings of the Separated Flow Past a Wing-Body
Combination

REGION I REGION II REGION III

U_∞
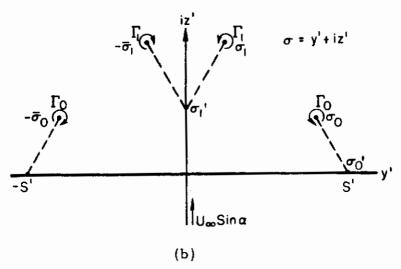
Figure 7. Distinct Cross-Flow Regimes for the General Wing-Body Configuration

37
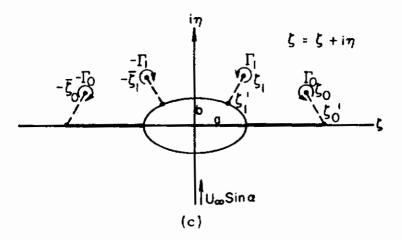
Figure 8. With Two Sets of Vortices, the Successive Flow
Past, (a), a Vertical Line, (b), a Horizontal Line,
and (c), Horizontal Line and an Ellipse

38
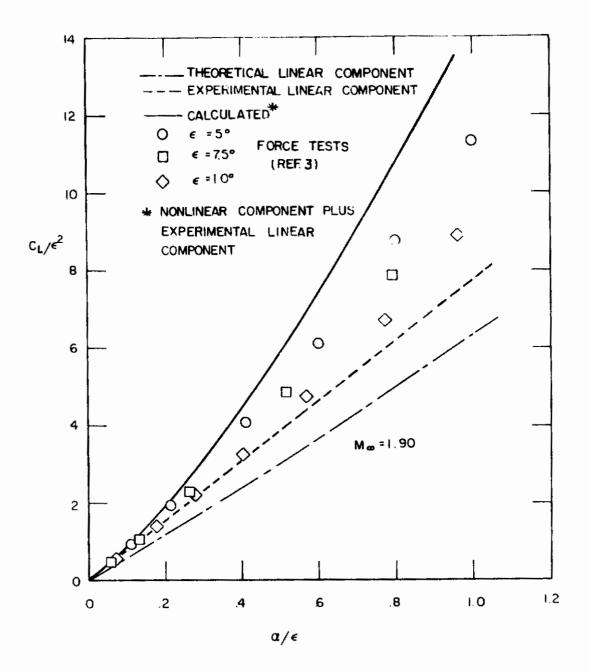
Figure 9. Comparison of Measured and Calculated Lift Results
On Delta Wings (Supersonic Flow)
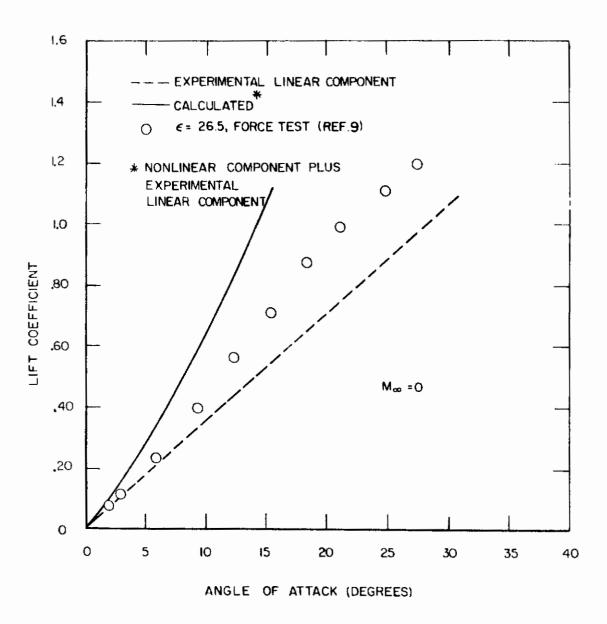
Figure 10. Comparison of Measured and Calculated Lift Results On Delta Wings (Subsonic Flow)
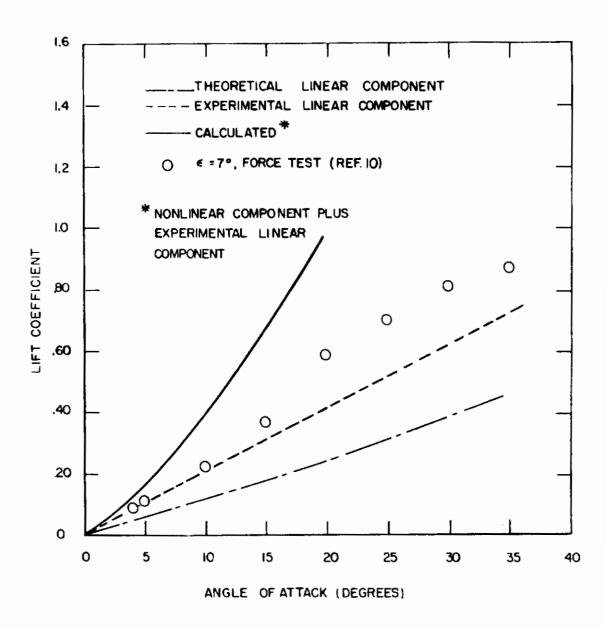
Figure 11. Comparison of Measured and Calculated Lift Results
On Delta Wings (Subsonic Flow)
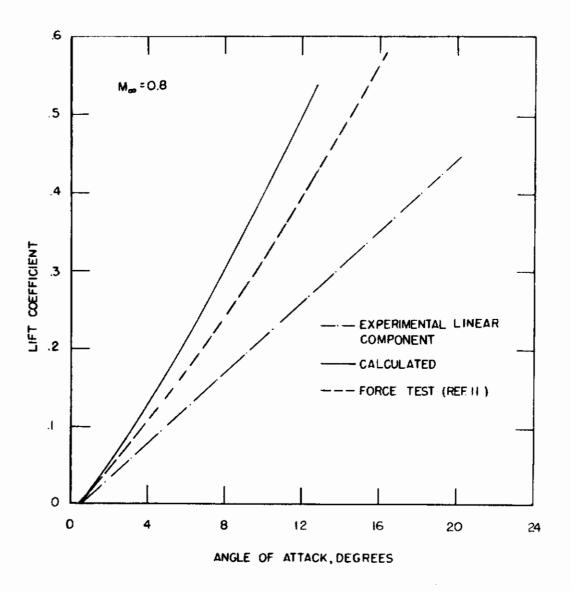
Figure 12. Comparison of Measured and Calculated Lift Results On Ogee Wings (Subsonic Flow)

42
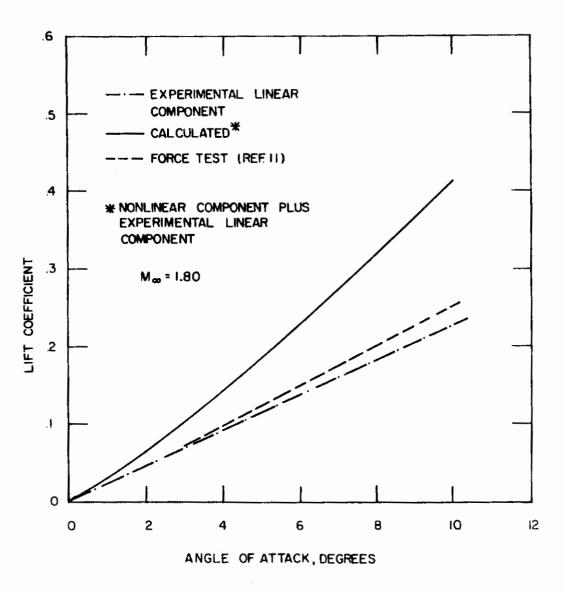
Figure 13.   Comparison of Measured and Calculated Lift Results on Ogee Wings (Supersonic Flow)
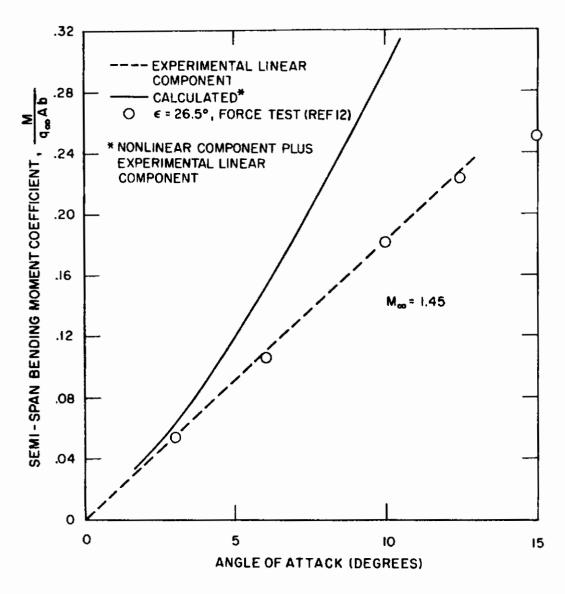
Figure 14. Comparison of Measured and Calculated Semi-Spanwise
Bending Moment for a Delta Wing
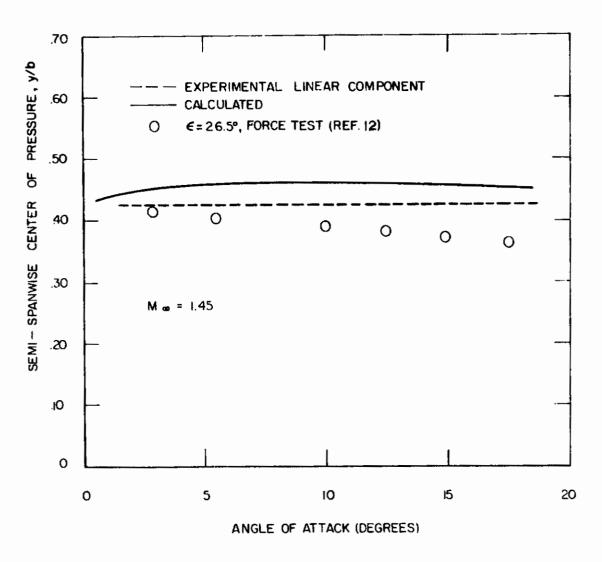
Figure 15. Comparison of Measured and Calculated Semi-Spanwise
Center of Pressure for a Delta Wing

45
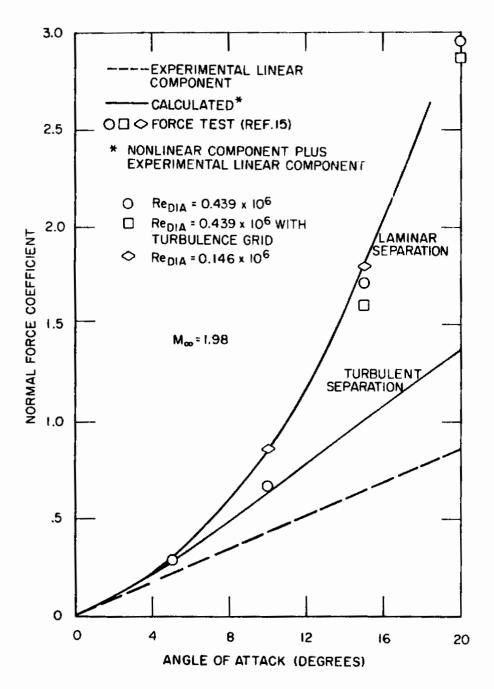
Figure 16. Comparison of Measured and Calculated Normal Force Coefficients for an Ogive-Cylinder

46
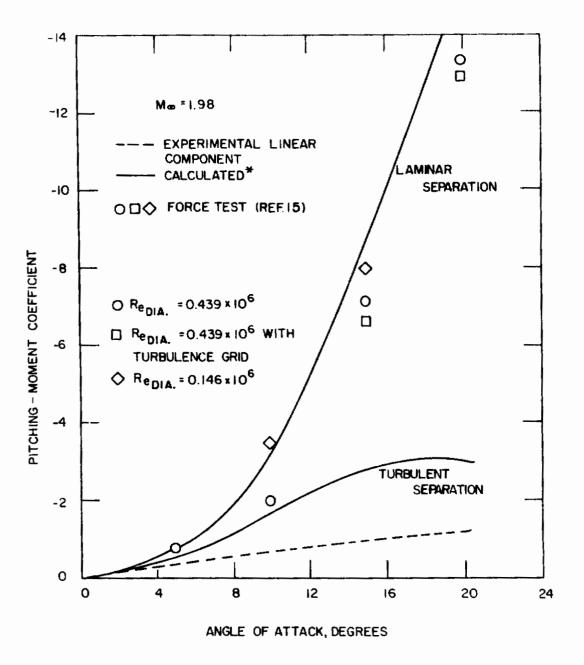
Figure 17. Comparison of Measured and Calculated Pitching Moment Coefficients for an Ogive-Cylinder

47

(a) $\alpha = 5°$
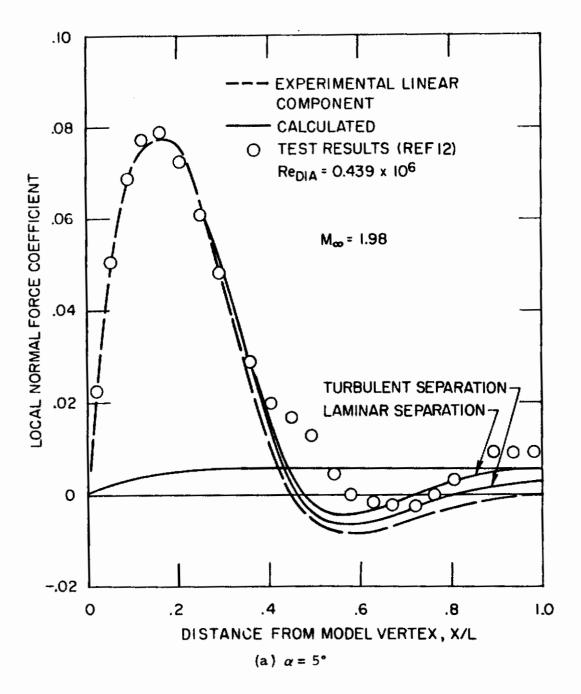
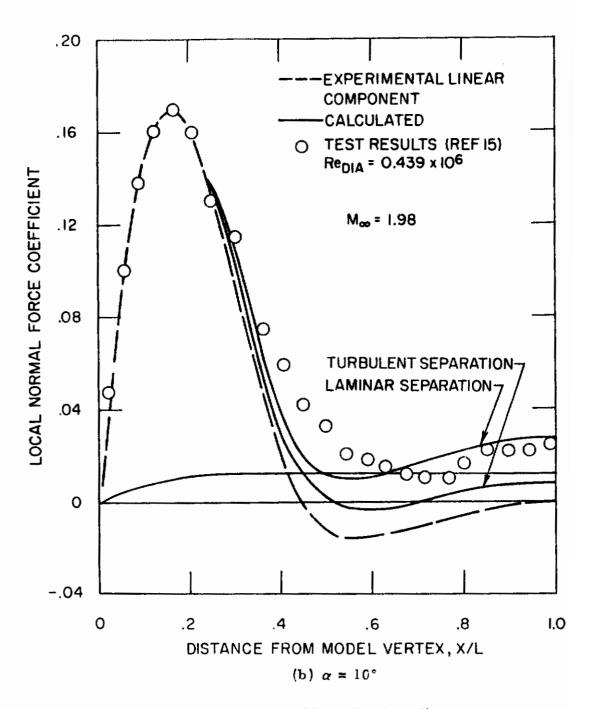Figure 18. Comparison of Calculated Normal Force Distributions with Experiment at Several Angles of Attack
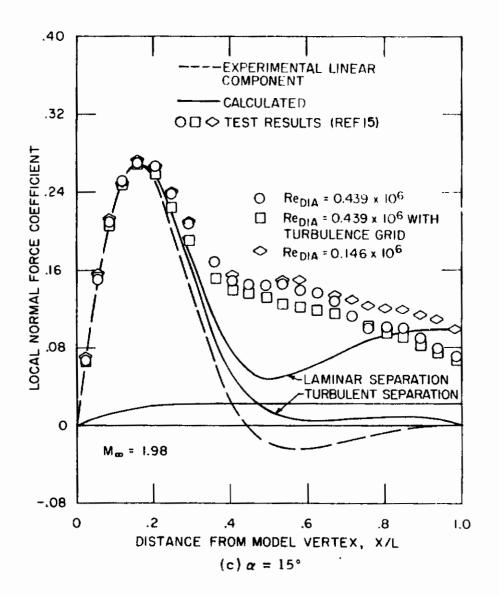
48

(b) $\alpha = 10°$

Figure 18. (Continued)
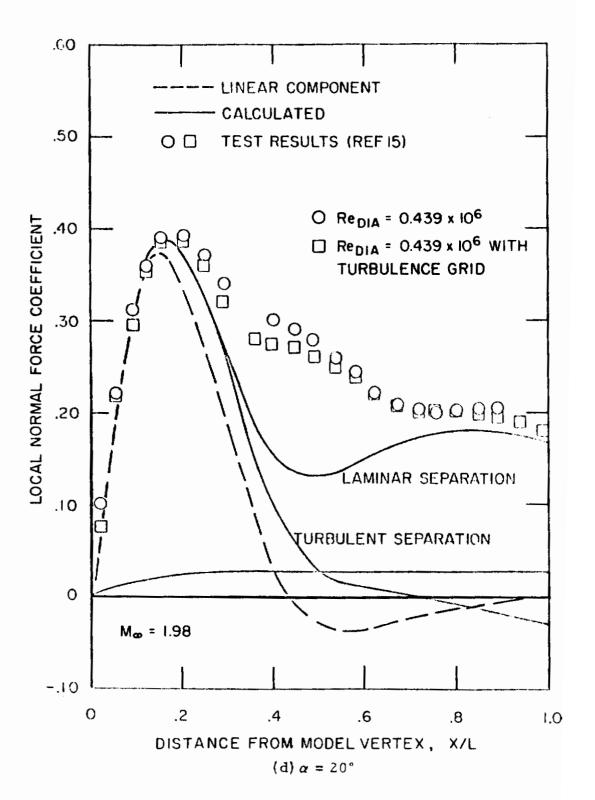
49

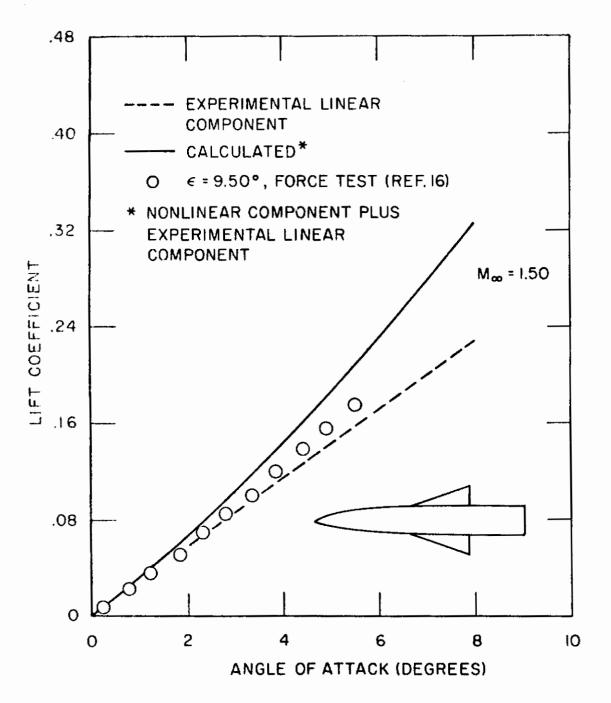Figure 18. (Continued)

Figure 18. (Concluded)

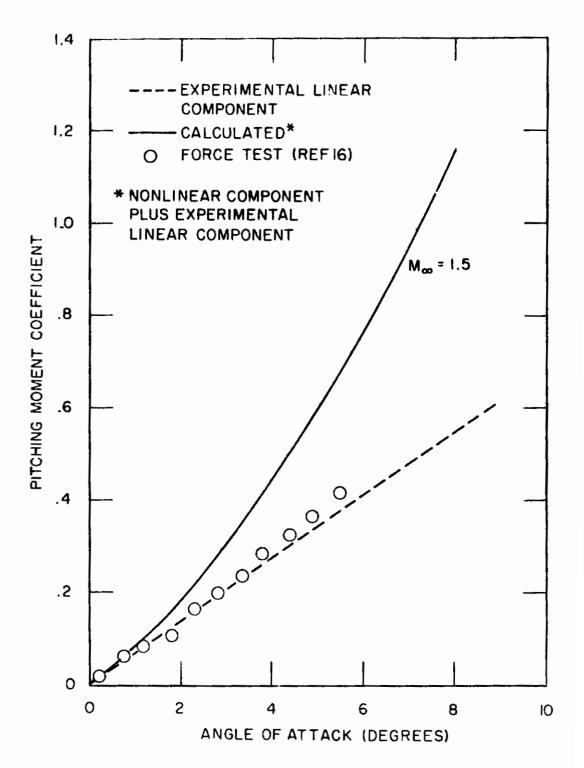Figure 19. Comparison of Measured and Calculated Lift Results for a Wing-Body Combination

Figure 20.   Comparison of Measured and Calculated Pitching
             Moments for a Wing-Body Combination

DOCUMENT CONTROL DATA - R&D

(Security classification of title, body of abstract and indexing annotation must be entered when the overall report is classified)

1. ORIGINATING ACTIVITY (Corporate author)	2a. REPORT SECURITY CLASSIFICATION
Massachusetts Institute of Technology 560 Memorial Drive Cambridge, Massachusetts	Unclassified
	2b. GROUP

3. REPORT TITLE

METHODS OF CALCULATING AERODYNAMIC LOADS ON AIRCRAFT STRUCTURES: PART II – NONLINEAR EFFECTS

4. DESCRIPTIVE NOTES *(Type of report and inclusive dates)*

Final Report; January 4, 1965 – January 3, 1966

5. AUTHOR(S) *(Last name, first name, initial)*

Chamberlain, Thomas E

6. REPORT DATE	7a. TOTAL NO. OF PAGES	7b. NO. OF REFS
August 1966	53 + ix	16

8a. CONTRACT OR GRANT NO. AF 33(615)-2291	9a. ORIGINATOR'S REPORT NUMBER(S)
b. PROJECT NO. 1367	AFFDL-TR-66-37, Part II
c. Task No. 136715	9b. OTHER REPORT NO(S) (Any other numbers that may be assigned this report)
d.	TR 126

10. AVAILABILITY/LIMITATION NOTICES

This document is subject to special export controls and each transmittal to foreign governments or foreign nationals may be made only with prior approval of Air Force Flight Dynamics Laboratory(FDTR), Wright-Patterson AFB, Ohio

11. SUPPLEMENTARY NOTES	12. SPONSORING MILITARY ACTIVITY
	Air Force Flight Dynamics Laboratory (FDTR), Wright-Patterson AFB, Ohio

13. ABSTRACT

A method is presented for analysis of the nonlinear aerodynamics of slender configurations with vortex separation. Primary emphasis is on the nonlinear component of the aerodynamic characteristics. The theory is intended to be mathematically tenable yet give results of acceptable accuracy.

A technique for analyzing the nonlinear aeroelastic problem is given followed by a method for obtaining the nonlinear aerodynamics of wings, bodies, and their combinations. Comparisons with experiment are provided.

The experimental comparisons with the wing results indicate that the theory overestimates the nonlinear forces at high angles of attack. The results indicate directions for further research.

DD FORM 1 JAN 64 **1473**

14. KEY WORDS	LINK A		LINK B		LINK C	
	ROLE	WT	ROLE	WT	ROLE	WT

INSTRUCTIONS

1. **ORIGINATING ACTIVITY:** Enter the name and address of the contractor, subcontractor, grantee, Department of Defense activity or other organization (*corporate author*) issuing the report.

2a. **REPORT SECURITY CLASSIFICATION:** Enter the overall security classification of the report. Indicate whether "Restricted Data" is included. Marking is to be in accordance with appropriate security regulations.

2b. **GROUP:** Automatic downgrading is specified in DoD Directive 5200.10 and Armed Forces Industrial Manual. Enter the group number. Also, when applicable, show that optional markings have been used for Group 3 and Group 4 as authorized.

3. **REPORT TITLE:** Enter the complete report title in all capital letters. Titles in all cases should be unclassified. If a meaningful title cannot be selected without classification, show title classification in all capitals in parenthesis immediately following the title.

4. **DESCRIPTIVE NOTES:** If appropriate, enter the type of report, e.g., interim, progress, summary, annual, or final. Give the inclusive dates when a specific reporting period is covered.

5. **AUTHOR(S):** Enter the name(s) of author(s) as shown on or in the report. Enter last name, first name, middle initial. If military, show rank and branch of service. The name of the principal author is an absolute minimum requirement.

6. **REPORT DATE:** Enter the date of the report as day, month, year; or month, year. If more than one date appears on the report, use date of publication.

7a. **TOTAL NUMBER OF PAGES:** The total page count should follow normal pagination procedures, i.e., enter the number of pages containing information.

7b. **NUMBER OF REFERENCES:** Enter the total number of references cited in the report.

8a. **CONTRACT OR GRANT NUMBER:** If appropriate, enter the applicable number of the contract or grant under which the report was written.

8b, 8c, & 8d. **PROJECT NUMBER:** Enter the appropriate military department identification, such as project number, subproject number, system numbers, task number, etc.

9a. **ORIGINATOR'S REPORT NUMBER(S):** Enter the official report number by which the document will be identified and controlled by the originating activity. This number must be unique to this report.

9b. **OTHER REPORT NUMBER(S):** If the report has been assigned any other report numbers (*either by the originator or by the sponsor*), also enter this number(s).

10. **AVAILABILITY/LIMITATION NOTICES:** Enter any limitations on further dissemination of the report, other than those imposed by security classification, using standard statements such as:

   (1) "Qualified requesters may obtain copies of this report from DDC."

   (2) "Foreign announcement and dissemination of this report by DDC is not authorized."

   (3) "U. S. Government agencies may obtain copies of this report directly from DDC. Other qualified DDC users shall request through
                        ."

   (4) "U. S. military agencies may obtain copies of this report directly from DDC. Other qualified users shall request through
                        ."

   (5) "All distribution of this report is controlled. Qualified DDC users shall request through
                        ."

If the report has been furnished to the Office of Technical Services, Department of Commerce, for sale to the public, indicate this fact and enter the price, if known.

11. **SUPPLEMENTARY NOTES:** Use for additional explanatory notes.

12. **SPONSORING MILITARY ACTIVITY:** Enter the name of the departmental project office or laboratory sponsoring (*paying for*) the research and development. Include address.

13. **ABSTRACT:** Enter an abstract giving a brief and factual summary of the document indicative of the report, even though it may also appear elsewhere in the body of the technical report. If additional space is required, a continuation sheet shall be attached.

It is highly desirable that the abstract of classified reports be unclassified. Each paragraph of the abstract shall end with an indication of the military security classification of the information in the paragraph, represented as (TS), (S), (C), or (U).

There is no limitation on the length of the abstract. However, the suggested length is from 150 to 225 words.

14. **KEY WORDS:** Key words are technically meaningful terms or short phrases that characterize a report and may be used as index entries for cataloging the report. Key words must be selected so that no security classification is required. Identifiers, such as equipment model designation, trade name, military project code name, geographic location, may be used as key words but will be followed by an indication of technical context. The assignment of links, rules, and weights is optional.

GPO 886-551